Hindawi
Advances in Civil Engineering
Volume 2018, Article ID 7208031, 12 pages
https://doi.org/10.1155/2018/7208031

Research Article

Seismic Performance of a Corroded Reinforce Concrete Frame Structure Using Pushover Method

Meng Zhang[1], **Ran Liu**[1], **Yaoliang Li**[1,2] **and Guifeng Zhao**[1]

[1]*School of Civil Engineering, Zhengzhou University, Zhengzhou 450001, China*
[2]*Liuzhou Administration of Power Supply of Guangxi Grid Company, China Southern Power Grid, Liuzhou 545005, China*

Correspondence should be addressed to Guifeng Zhao; gfzhao@zzu.edu.cn

Received 7 January 2018; Revised 17 March 2018; Accepted 1 April 2018; Published 2 May 2018

Academic Editor: Song Han

SAP2000 software was used to build the finite element model of a six-storey-three-span reinforced concrete (RC) frame structure. The numerical simulation of the seismic performance of the RC frame structure incorporating different levels of rebar corrosion was conducted using pushover analysis method. The degradation characteristics of the seismic performance of the corroded structure under severe earthquake were also analyzed. The results show that the seismic performance of the RC frame decreased significantly due to corrosion of the longitudinal rebars. And the interstory drift ratios increase dramatically with the increasing of the corrosion rate. At the same time, the formation and development of plastic hinges (beam hinges or column hinges) will accelerate, which leads to a more aggravated deformation of the structure under rare earthquake action, resulting in a negative effect to the seismic bearing capacity of the structure.

1. Introduction

The building seismic fortification requirements are gradually improving around the world, and the buildings in strict accordance with design and construction code also showed good seismic performance during earthquakes. But in recent years, the houses collapses, highway cracks [1], and casualties caused by earthquakes are still high, such as the Wenchuan earthquake, the India-Pakistan earthquake [2], and the Chilean earthquake [3]. The postdisaster survey data show that collapsed or severely damaged houses are mainly multistorey masonry buildings or concrete frame structures with relatively poor seismic performance [4].

Currently, multistory masonry houses have been gradually restricted to be built and used in large and medium-sized cities, while the reinforced concrete frame buildings are still widely used in schools, office buildings, residential buildings, street shops, and other buildings due to their flexible plan layout and strong adaptability. With the increase of service years, under the induction of external corrosion factors, the material of reinforced concrete frame structure will deteriorate [5–8], resulting in the durability damage (such as surface cracks [9], carbonization, spalling, and steel corrosion [10]). Among which, the corrosion of steel bar is regarded as the prime factor that affecting the durability of concrete structures [11–13]. Corrosion leads to the degradation of geometric parameters and mechanical properties of the rebar and, to some extent, weaken the static bearing capacity of a concrete structure and increase its brittleness. Meanwhile, the seismic performance will be inevitably impaired [14–17]. Therefore, it is of important theoretical significance and engineering guiding value to study the degradation law of seismic performance of corroded reinforced concrete frame structures. At the same time, it can also provide reference about the seismic performance evaluation and maintenance reinforcement for the old reinforced concrete frame structures in the seismic area.

In this paper, the finite element model of a six-storey-three-span corroded reinforced concrete (RC) frame structure was built using SAP2000 software [18, 19]. The numerical simulation of the seismic performance of the corroded RC frame structure was conducted using pushover analysis method [20] because pushover analysis method is the most widely used and convenient method for the seismic performance analysis of the middle-low level RC frame structure. Pushover method is based on the structural static

elastic-plastic analysis theory, by increasing the lateral load on the inertial force center of each floor of the structure to obtain the relationship between internal forces and deformation response in this process. Finally, using the seismic demand spectrum and capacity spectrum (ATC-40 response spectrum or Chinese code response spectrum) to estimate the performance point index of the structure, one can easily evaluate the seismic performance of the structure [21]. The main advantage of the pushover analysis method is that the elastic-plastic response of the structure can be considered and the calculation results are stable. This paper also analyzed the degradation law of the seismic performance indicators of the corroded RC frame structure under severe earthquake. The results were expected to provide a reference for seismic safety analysis, reliability assessment, maintenance reinforcement, and reconstruction of corroded RC frame structures.

2. Mechanical Properties of Corroded Reinforced Concrete Materials

2.1. Degradation of the Mechanical Properties of Concrete Cover. A large number of experiments and theoretical analyses have shown that the concrete cover of a RC frame structure will be cracked and peeled off due to the role of rust expansion force after the steel corrosion. In addition, it weakens the bond strength between the rebar and concrete, hence reducing the service life of the structure [22, 23]. Considering that the core concrete binding force of an ordinary reinforced cement concrete member is mainly from the protective layer, the cracking and peeling of the concrete cover will reduce its restraint on the core concrete and further weaken the load and deformation capacity of the member. Therefore, the degradation of mechanical properties of the protective concrete cover should not be ignored during structural analysis. Due to the strong random characteristics of the deterioration of the cover concrete, it is difficult to use analytic methods to determine the degree and location of deterioration. In order to simplify the calculation, (1) is used here to calculate the strength of the cover concrete [24, 25].

$$\begin{aligned} f_{\mathrm{c-cor}} &= \frac{f_{\mathrm{c}}}{1+\gamma\left(\varepsilon_{\mathrm{t\text{-}cor}}/\varepsilon_{\mathrm{c}}\right)}, \\ \varepsilon_{\mathrm{t-cor}} &= \frac{b_{\mathrm{cor}}-b}{b}, \\ b_{\mathrm{cor}} &= b+n\omega_{\mathrm{cor}}, \\ \omega_{\mathrm{cor}} &= \sum_{i} u_{i\mathrm{cor}} = 2\pi\left(v_{\mathrm{cor}}-1\right)X, \\ \rho_{\mathrm{s}} &= \frac{2X}{r}-\left(\frac{X}{r}\right)^{2}, \end{aligned} \tag{1}$$

where $f_{\mathrm{c-cor}}$ is the peak value of the compressive strength of the concrete cover after the steel bar corrosion; γ is the correlation coefficient between the rebar surface shape and its diameter, and it is usually suggested to be 0.1; $\varepsilon_{\mathrm{t-cor}}$ is the generalized cracking strain of concrete; b is the original width of the member; b_{cor} is the cross-sectional width of the corrosion member; n is the number of longitudinal rebars; ω_{cor} is the total width of the corrosion crack; v_{cor} is rust oxidation products and the volume ratio coefficient before rust, and it can be taken value 2.0; $u_{i\mathrm{cor}}$ is the width of the ith corrosion crack; X is the depth of steel bar corrosion; ρ_{s} is the corrosion loss rate of the rebar section; and r is the radius of the steel rebar before corrosion, and it can be taken as the weighted average value when the reinforcement diameters are different.

2.2. Degradation of the Corrosion Steel Bar Mechanical Properties. Usually, because the distribution of rust factors (such as cracks, chloride ions, and sulfate ions [26]) has significant random characteristics, the corrosion status of reinforcement in RC members often appears as pitting corrosion. Numerical analysis usually adopts the method of equivalent uniform corrosion to deal with the degradation of mechanical properties of pit corroded steel bars, so as to improve the accuracy of numerical simulation or theoretical analysis [27]. It is assumed that the cross section of the rebar is in a uniform corrosion state, but its mechanical properties are degradated according to the pit corrosion equation. In order to consider the effect of pitting corrosion on the mechanical properties of corroded rebar, the nominal yield stress and elastic modulus of the corroded rebar are calculated by (2) [28], and the ultimate stress and strain [29] can be calculated by (3).

$$\begin{aligned} f_{\mathrm{yc}} &= (1-0.0198\delta)f_{\mathrm{y}}, \\ E_{\mathrm{sc}} &= (1-0.0113\delta)E_{\mathrm{s}}, \end{aligned} \tag{2}$$

$$\begin{aligned} f_{\mathrm{uc}} &= (1.0-0.019\delta)f_{\mathrm{u}}, \\ \varepsilon_{\mathrm{uc}} &= (1.0-0.021\delta)\varepsilon_{\mathrm{u}}, \end{aligned} \tag{3}$$

where f_{y} (f_{yc}) is the nominal yield strength of the steel bar before (after) corrosion; E_{s} (E_{sc}) is the nominal modulus of elasticity of the steel bar before (after) corrosion; f_{u} (f_{uc}) is the nominal ultimate strength of the steel bar before (after) corrosion; ε_{u} ($\varepsilon_{\mathrm{uc}}$) is the nominal ultimate strain of the steel bar before (after) corrosion; and δ stands for the mass loss rate of the corroded steel. The relationship between ρ_{s} and δ can be seen in (4) [28].

$$\rho_{\mathrm{s}} = \begin{cases} 0.013+0.987\delta, & \delta \le 10\% \\ 0.061+0.939\delta, & 10\% < \delta \le 20\% \\ 0.129+0.871\delta, & 20\% < \delta \le 30\% \\ 0.199+0.810\delta, & 30\% < \delta \le 40\% \end{cases} \tag{4}$$

3. Pushover Analysis Results of the Noncorroded RC Frame Structure

3.1. Engineering Background and Calculation Parameters. For the purposes of comparison, a model of noncorroded RC frame building was presented here. The building model has six stories with typical story height 3.6 m, and the overall plan area is 24×12 m. All beams are 300×550 mm. The columns in 1–3 storeys are 500×500 mm, while the columns

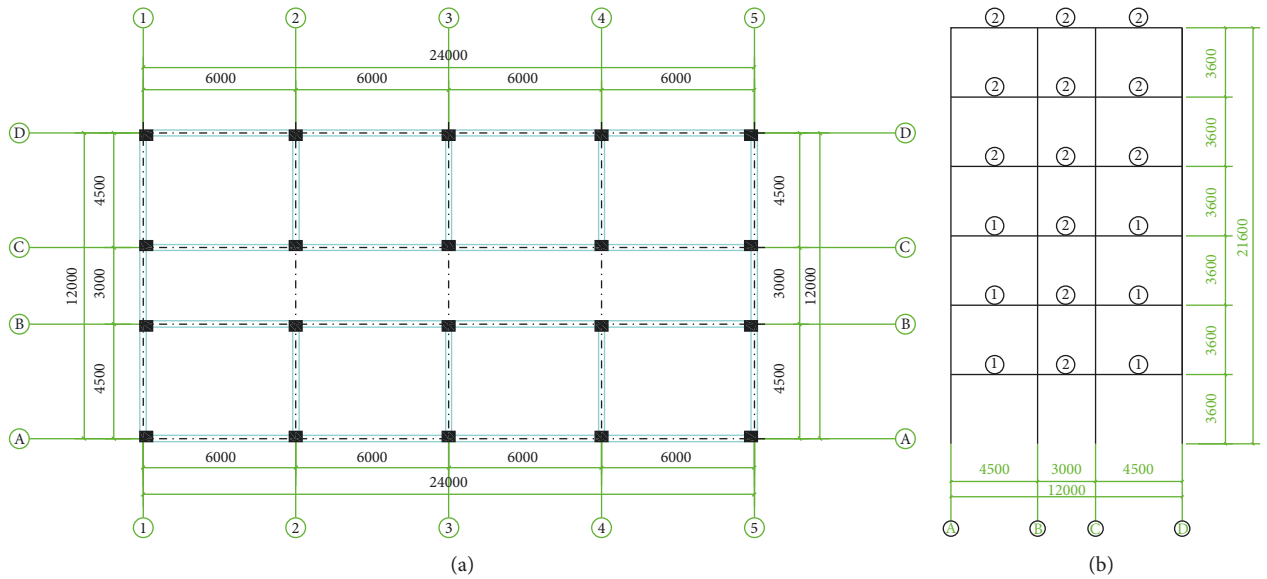

(a) (b)

Figure 1: Layout of the RC frame building. (a) Plane of the RC frame structure. (b) Elevation of the RC frame structure in axis ③-③.

Table 1: Representative values of the gravity load on the RC frame.

	Distributed span load (kN/m)		Concentrated load (kN)	
	Beam in side span	Beam in middle span	Node in side span	Node in middle span
Standard storeys	22.9	11.3	111.4	122.8
Top storey	18.2	12.1	78.3	151.9

in 4–6 storeys are 400 × 400 mm, rectangular. Figure 1 shows the typical structural layout. It can be seen that the building model is a typical biaxially symmetric structure. Therefore, to simplify the following computation, only the plane frame in axis ③-③ (Figure 1(b)) is selected to perform pushover analysis.

According to Chinese Standard GB50011-2010, Code for Seismic Design of Buildings [30], the building is located in class II site, with the design earthquake group of 2, and the design basic acceleration of ground motion 0.20 g. The loads acting on the building are in strict accordance with Chinese Standard GB50009-2012, Load Code for the Design of Building Structures [31], and the representative values of the gravity load are shown in Table 1.

The design strength of concrete was C30 grade, and the longitudinal reinforcement was Grade II rebar (HRB335), while Grade I rebar (HPB300) was used for the stirrups. Figure 2 shows the geometric parameters and the reinforcement layout of the beams and columns. The detailed design material parameters and reinforcement parameters of the beams and columns are shown in Tables 2 and 3, respectively.

3.2. Pushover Analysis Method. Pushover analysis is a static-nonlinear analysis method [20]. During pushover analysis, a structure is subjected to lateral load which continuously increases through elastic and inelastic behaviours until the ultimate condition is reached. The key thing here is that the plastic hinge theory plays an important role in pushover analysis. Plastic hinges are often used to simulate the nonlinear behaviour of the structure; the plastic development degree of the plastic hinges is used to reflect the plastic development degree of the structure. In the SAP2000 program, yielding and postyielding behaviour can be modelled using either default hinges or user-defined hinges. Each hinge represents concentrated postyield behaviour in one or more degrees of freedom. Default hinges include uncoupled moment (M), torsion (T), axial force (P), shear (V) hinges, and coupled P-M2-M3 (or P-M-M) hinge which yields based on the interaction of axial force and bending moments at the hinge location. For the P-M-M hinge, an interaction (yield) surface should be specified in the three-dimensional P-M2-M3 space that represents the first yielding location for different combinations of axial force P, minor moment M2, and major moment M3. In the SAP2000 program, the built-in default hinge properties for steel members are provided based on FEMA-356 criteria [32], and the built-in default hinge properties for concrete members are generally based on ATC-40 criteria [33]. For the user-defined plastic hinges, XTRACT [34] software is generally utilized to determine the moment-rotation curves for beam and P-M-M interaction curves for columns. When analyzing an RC frame structure, plastic hinge regions are usually assigned to the ends of the members. For the beam element, the plastic hinge is usually yielded only by the bending moment (M), and the plastic hinge is generally considered by the axial force and the two-way bending moment correlation (P-M-M) for the column element. When the default hinge is adopted to simulate the

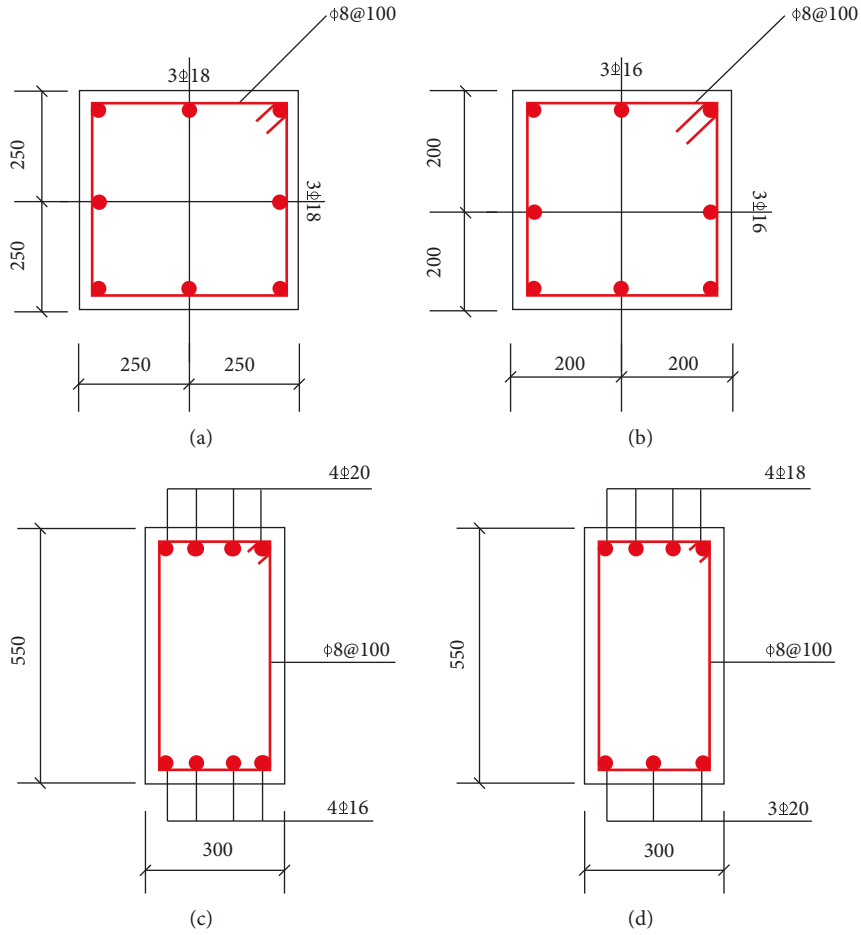

Figure 2: Dimensions and reinforcement layout of the RC frame members. (a) Reinforcement layout of columns in 1–3 storey. (b) Reinforcement layout of columns in 4–6 storey. (c) Reinforcement layout of beams ① (Figure 1(b)). (d) Reinforcement layout of beams ② (Figure 1(b)).

Table 2: Material parameters of noncorroded members.

Concrete (C30)	f_{cu} (MPa)	f_c (MPa)	f_t (MPa)	E_c (MPa)
	30	24	2.4	24595.2
Longitudinal reinforcement (HRB335)	f_y (MPa)	f_u (MPa)	ε_u	E_s (MPa)
	335	455	0.15	200000

Table 3: Detailed reinforcement parameters of beams and columns.

Column reinforcement (mm^2)	Beam reinforcement (mm^2)			
Storey	—	Beam numbering	Upper reinforcement	Bottom reinforcement
1–3	2036	①	1256	804
4–6	1608	②	1017	942

nonlinear behavior of the structure, only the influence of rebar corrosion on degradation law of the plastic hinge parameters can be considered. However, from the above analysis, it can be seen that the degradation of mechanical properties of the protective concrete cover should not be ignored during the structural analysis. The user-defined hinge can fully consider the effects of rebar corrosion and the degradation of mechanical properties of the protective concrete cover as well as the plastic hinge parameters degradation law, so we adopt a user-defined plastic hinges in the nonlinear analysis of the structure.

To determine the development of the plastic hinges on the frame structure, a force-displacement (moment-rotation) curve can be defined according to FEMA-356 criteria, which gives the yield value and the plastic deformation following yield. This is done in terms of a curve with values at five points, A-B-C-D-E, as shown in Figure 3.

As is suggested by Figure 3, there are four line segments (i.e., AB, BC, CD, and DE) in the skeleton curve, representing the elastic stage, the strengthening stage, the unloading stage, and the failure stage, respectively. Moreover, FEMA-356 criteria also set three performance points (i.e., IO, LS, and CP) between the characteristic points B and C. IO is the abbreviation for "Immediate Occupancy," which means that the structure is in the serviceability limit state. LS is the abbreviation for "Life Safety," which means that the structure is close to the safety limit state. CP is the

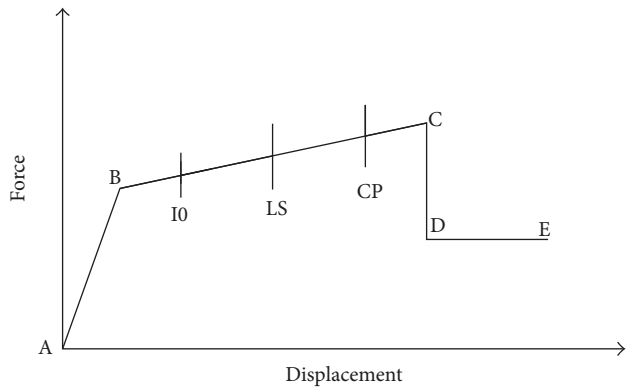

Figure 3: Typical nonlinear skeleton curve in SAP2000 according to FEMA-356.

abbreviation for "Collapse Prevention," which means that the structure is close to the collapse limit state.

3.3. Pushover Analysis Results

3.3.1. Comparison of the P-M-M Curves between Default Hinges and User-Defined Plastic Hinges. In view of the biaxial symmetry of the cross section of the noncorroded frame column, Figure 4 presents only the correlation curve of the axial force P and the major moment M3 in the x direction of the column section. It can be seen that the P-M-M curves obtained by user-defined plastic hinge are in good agreement with those by the built-in default hinge in SAP2000 software.

Table 4 provides the parameters of the P-M-M curves of the noncorroded column section. It can be seen from Figure 4 and Table 4 that the computed key-point parameters of the P-M-M curves using user-defined hinge are generally consistent with those acquired by the built-in default hinge in SAP2000 software. The maximum discrepancy is within 5%. This indicated that the user-defined hinge has relatively higher precision and can be used in the subsequent analysis.

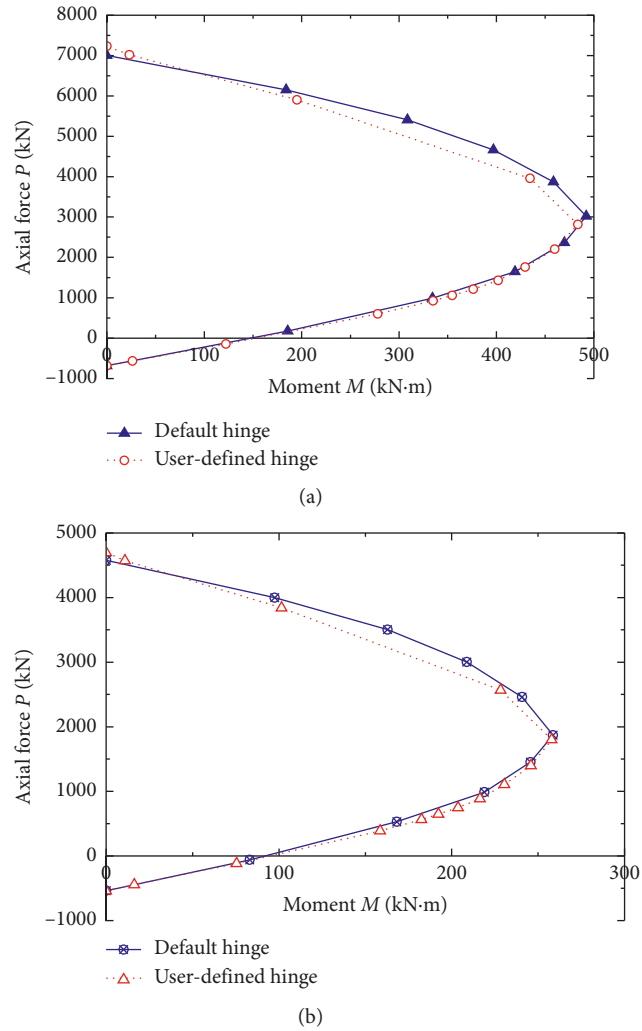

Figure 4: Comparison of the P-M-M curves of the noncorroded RC column section. (a) RC column with cross section of 500 × 500 mm. (b) RC column with cross section of 400 × 400 mm.

3.3.2. Comparison of the Pushover Analysis Results between Default Hinges and User-Defined Hinges. Considering that the load pattern may affect the pushover analysis results dramatically, it is important to consider at least two different lateral pushover cases to represent different sequences of response that could occur during dynamic loading [29]. Therefore, the pushover analysis in this paper should be performed using both of the following lateral load patterns: the uniform pattern, corresponding to uniform unidirectional lateral acceleration; and the 1st modal pattern. The 1st modal pattern is a pattern of forces on the joints that is proportional to the product of the fundamental mode shape times its circular frequency squared times the mass tributary to the joint. In view of the remarkable material nonlinear of concrete, the load pattern based on displacement control is chosen in this paper to avoid trouble converging. The pushover curves for the plane frame in axis ③-③ under different load patterns are shown in Figure 5.

From the simulation results in Figure 5, we can see that although the pushover curves of the frame are quite different under different lateral load patterns, the pushover curves obtained by using user-defined hinges almost exactly coincide with those by using the default plastic hinges in SAP2000 under the same lateral load pattern.

Table 5 gives the calculation results of the elastoplastic interstory drift ratios of the noncorroded plane frame under rare earthquake action. From Table 5, it could also be seen that the story drift ratios obtained by using user-defined hinges are generally consistent with those obtained by using the default hinges in SAP2000 under the same lateral load pattern. The maximum discrepancy is less than 5%, and the maximum story drift ratio is very close to 1/120, which can meet the code requirement [32].

4. Pushover Analysis Results of the Corroded Frame Structure

4.1. Plastic Hinge Properties of Corroded Beams and Columns. When considering rebar corrosion, the geometric parameters and mechanical properties of the rebar will degenerate, which will inevitably affect the plastic hinge properties of

Table 4: Parameters of the key points of the P-M-M curves of the RC frame column.

	Maximum compression force (kN)	Maximum tension force (kN)	Maximum bending moment (kN·m)
(a) Column with cross section of 500 × 500 mm			
Default hinge (i)	7005.1	682.3	492.3
User-defined hinge (ii)	7231.0	682.0	483.7
Relative error (%) ((ii) − (i)/(i)) × 100%	3.22	−0.04	−1.75
(b) Column with cross section of 400 × 400 mm			
Default hinge (i)	4577.4	538.8	258.6
User-defined hinge (ii)	4697.0	538.8	257.9
Relative error (%) ((ii) − (i)/(i)) × 100%	2.61	0	-0.27

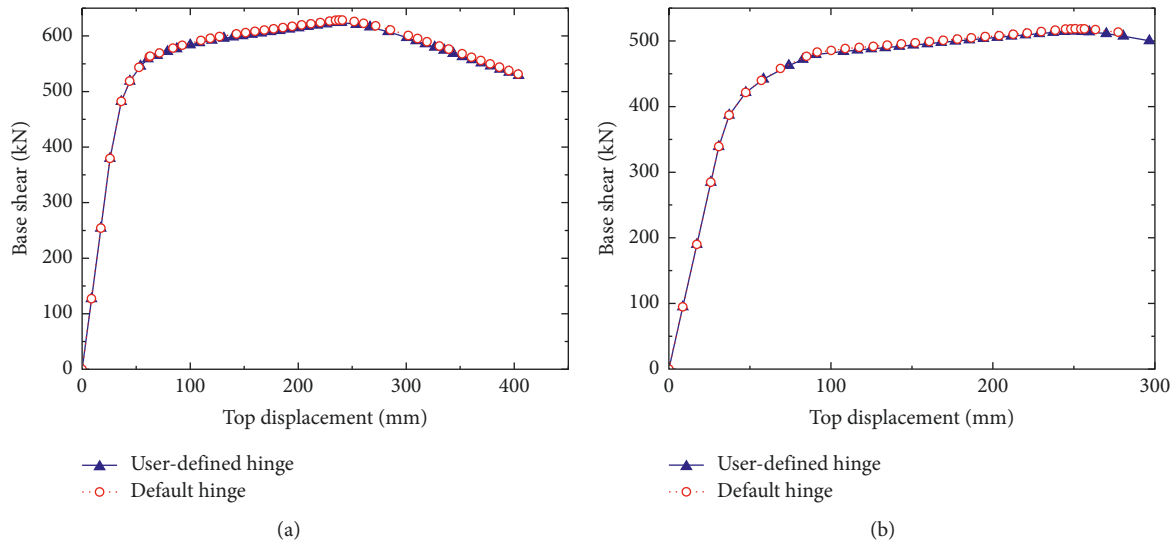

Figure 5: Comparison of the pushover curves of the noncorroded RC frame under different load patterns. (a) Under the uniform load pattern. (b) Under the 1st modal load pattern.

corroded beam and columns. To simplify the following computation, in this paper, the P-M-M interaction curves for different corroded RC columns are calculated using user-defined hinge with the help of XTRACT software, while the moment curvature (M3) for different corroded RC beams can be obtained using user-defined hinge by literature [35].

To understand the influence of different amounts of rebar corrosion on the seismic performance of the RC frame structure, four sets of operating conditions, including non-corroded, slight corrosion, moderate corrosion, and severe corrosion, were selected. According to the literature [35], the corresponding uniform corrosion rates of the rebar cross section under the four conditions above were 0%, 5%, 10%, and 18%, respectively. The corresponding concrete cover and reinforcement parameters under the four cases, including the strength of concrete cover, the yield strength of the rebar, the elastic modulus of the rebar, etc., are listed in Table 6.

4.1.1. Degradation of the P-M-M Curves of Corroded Column Using User-Defined Hinge. According to the parameters in Table 6, the P-M-M curves of the RC column under different degrees of corrosion can be obtained, and the results are shown in Figure 6. It can be seen that with an increased corrosion rate, the ultimate bearing capacity of compression, tension, and bending of the frame column section decreased after the rebar corrosion. However, comparatively speaking, the ultimate bending moment of the section deteriorates observably. Table 7 shows the detailed results of the

Table 5: Story drift ratios of the noncorroded plane frame under rare earthquake action.

Storey	Default hinge (i)	User-defined hinge (ii)	Relative error (%) ((ii) − (i)/(i)) × 100%
(a) Under the uniform load pattern			
1	1/162.3	1/163.9	−0.97
2	1/125.9	1/126.1	−0.13
3	1/148.8	1/148.6	0.15
4	1/220.8	1/221.7	−0.44
5	1/574.6	1/565.0	1.72
6	1/1234.6	1/1219.5	1.23
(b) Under the 1st modal load pattern			
1	1/201.6	1/201.6	0.00
2	1/125.9	1/125.6	0.25
3	1/119.3	1/119.6	−0.24
4	1/137.2	1/140.3	−2.19
5	1/396.8	1/380.2	4.37
6	1/900.9	1/885.0	1.80

Table 6: Mechanical property parameters of corroded RC material under different degrees of corrosion.

(a) Strength of concrete cover				
Corrosion rate (%)	f_c (MPa)			
0.0	24.0			
5.0	16.7			
10.0	12.7			
18.0	9.2			
(b) Mechanical properties of corroded rebar				
Corrosion rate (%)	f_y (MPa)	f_u (MPa)	E_s (MPa)	ε_u
0.0	335.0	455.0	200000	0.15
5.0	299.8	409.1	188002	0.13
10.0	266.7	366.0	176739	0.12
18.0	214.1	297.5	158821	0.09

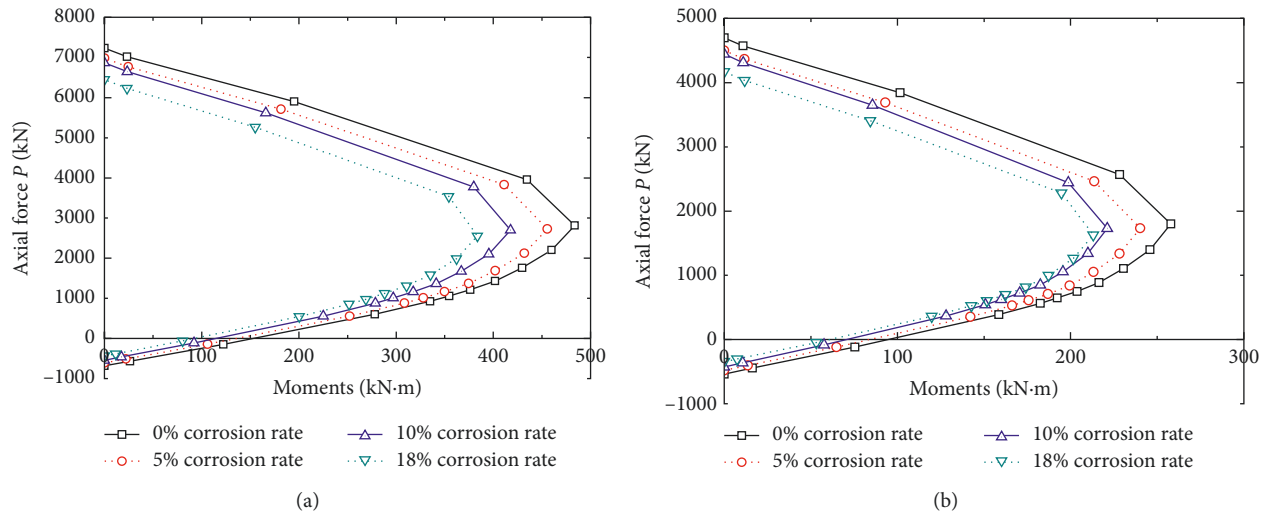

Figure 6: Comparison of the P-M-M curves of the column under different degrees of corrosion. (a) Column with cross section of 500 × 500 mm. (b) Column with cross section of 400 × 400 mm.

Table 7: Degradation of the ultimate bending moment of corroded column section.

Corrosion rate (%)	M_{max} (kN·m)	
	Column (500 × 500 mm)	Column (400 × 400 mm)
0.0	483.7	257.9
5.0	455.5	240.2
10.0	417.6	221.2
18.0	383.6	213.1

degradation of maximum bending moments under cases with different corrosion rates.

4.1.2. Degradation of the Bending Strength of Corroded Frame Beam. In this paper, the bending strength for noncorroded beam hinge (M3) can be computed using the built-in default hinge properties in SAP2000. For the plastic hinge properties of corroded beams, the bending strength of the beam hinge (M3) can be obtained with the help of the calculation results of literature [35]. The ultimate bending moment of corroded beams with four different amounts of corrosion are shown in Table 8.

Table 8: Bending strength of corroded beam hinge (M3) under different degrees of corrosion.

Corrosion rate (%)	Beam ①		Beam ②	
	$+M$ (kN·m)	$-M$ (kN·m)	$+M$ (kN·m)	$-M$ (kN·m)
0.0	129.9	198.8	151.3	162.8
5.0	118.1	180.7	137.5	148.0
10.0	103.4	158.2	120.4	129.5
18.0	74.0	113.3	86.2	92.8

$+M$ represents the bending strength of the bottom longitudinal reinforcement; $-M$ represents the bending strength of the upper longitudinal reinforcement.

4.2. Pushover Analysis Results for Corroded RC Frame. Generally, the corrosion of rebar in RC frame structures is mainly caused by carbonisation, cracking, and spalling of the concrete cover. Therefore, it can be reasonably assumed that the corrosion rates of columns and beams are the same [12]. On the base of the parameters for plastic hinge properties of corroded beams and columns in Figure 6 and Tables 6–8, the static pushover analysis under rare earthquake action was carried out incorporating inelastic material behaviour for concrete and steel with different corrosion rates.

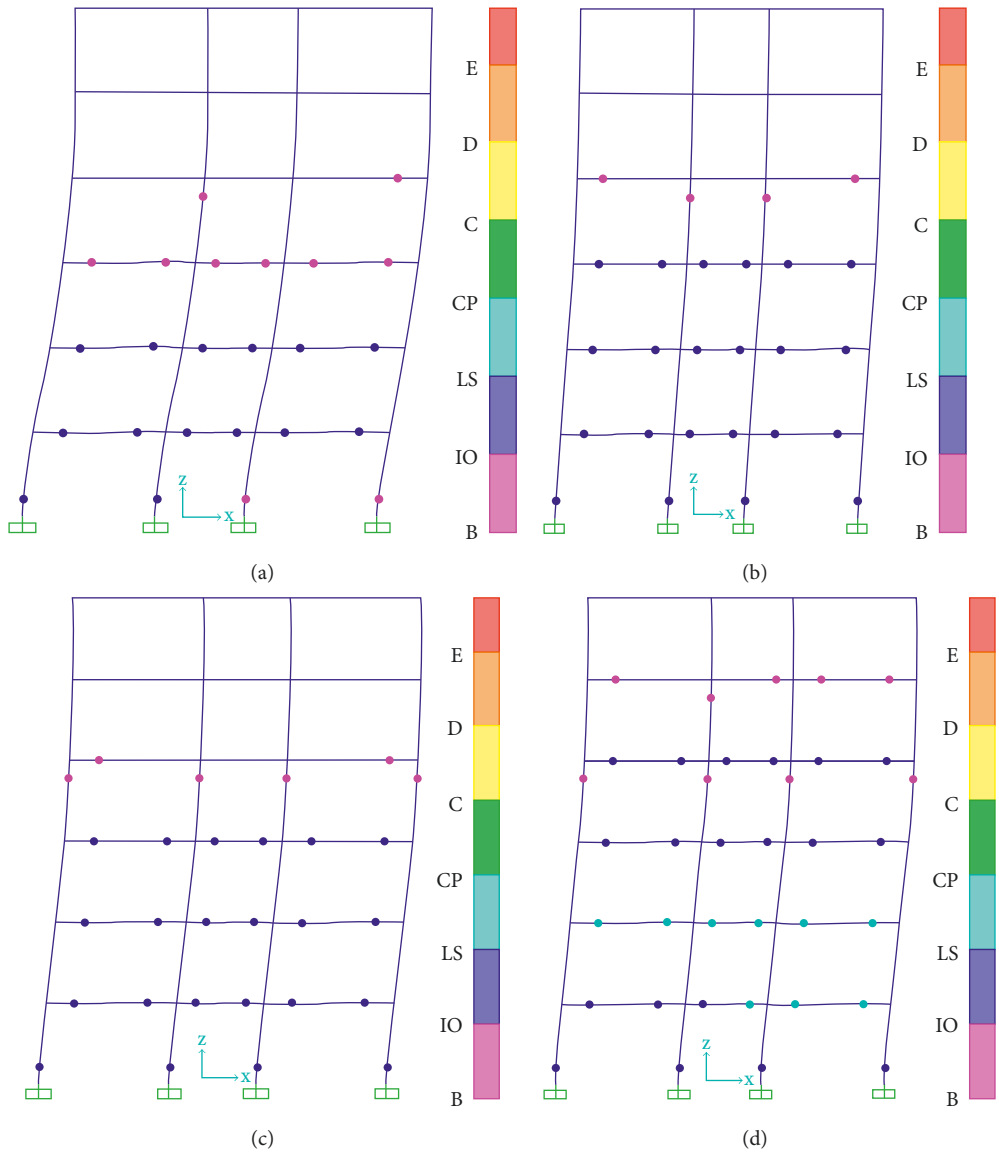

Figure 7: Distribution of plastic hinges under the uniform load pattern. (a) 0% corrosion rate. (b) 5% corrosion rate. (c) 10% corrosion rate. (d) 18% corrosion rate.

4.2.1. Plastic Hinges Formation and Development. Figures 7 and 8 show the distribution of plastic hinges for the corroded plane frame in axis ③-③ when the performance point (shown in Figure 3) is reached. As can be seen from the figures, with an increasing rebar corrosion rate, the number of plastic hinges in beams and columns increased gradually. Meanwhile, the hinges developed rapidly from the bottom to the higher storey with an increasing development level. Under slight corrosion condition (corrosion rate is less than 5%), the number and distribution of the plastic hinges for the corroded frame are approximately the same as that for the noncorroded frame (corrosion rate is equal to 0%). For moderately or seriously corroded frame, the number of plastic hinges increased significantly relative to the noncorroded structure, and the beam hinges have a large development rate than column hinges. By comparison, under the uniform lateral load pattern, the development degree of the plastic hinges for the same corroded frame is higher than that under the 1st modal load pattern.

As shown in Figures 7 and 8, there are 6 segments (i.e., B-IO, IO-LS, LS-CP, CP-C, C-D, and D-E) in the legend band. Each legend band is represented by a different colour, which can help the reader to judge the damage state of the structure or member. For example, it can be seen from the frame figure that there are pink points, blue points, and green points in the frame beams and columns, which are distributed in the B-IO segment, IO-LS segment, and LS-CP segment of the legend band, respectively. Therefore, according to the explanation shown in Figure 3, we can determine the stress states of these points as the serviceability stage, the safety stage, and the prevention of the collapse stage, respectively.

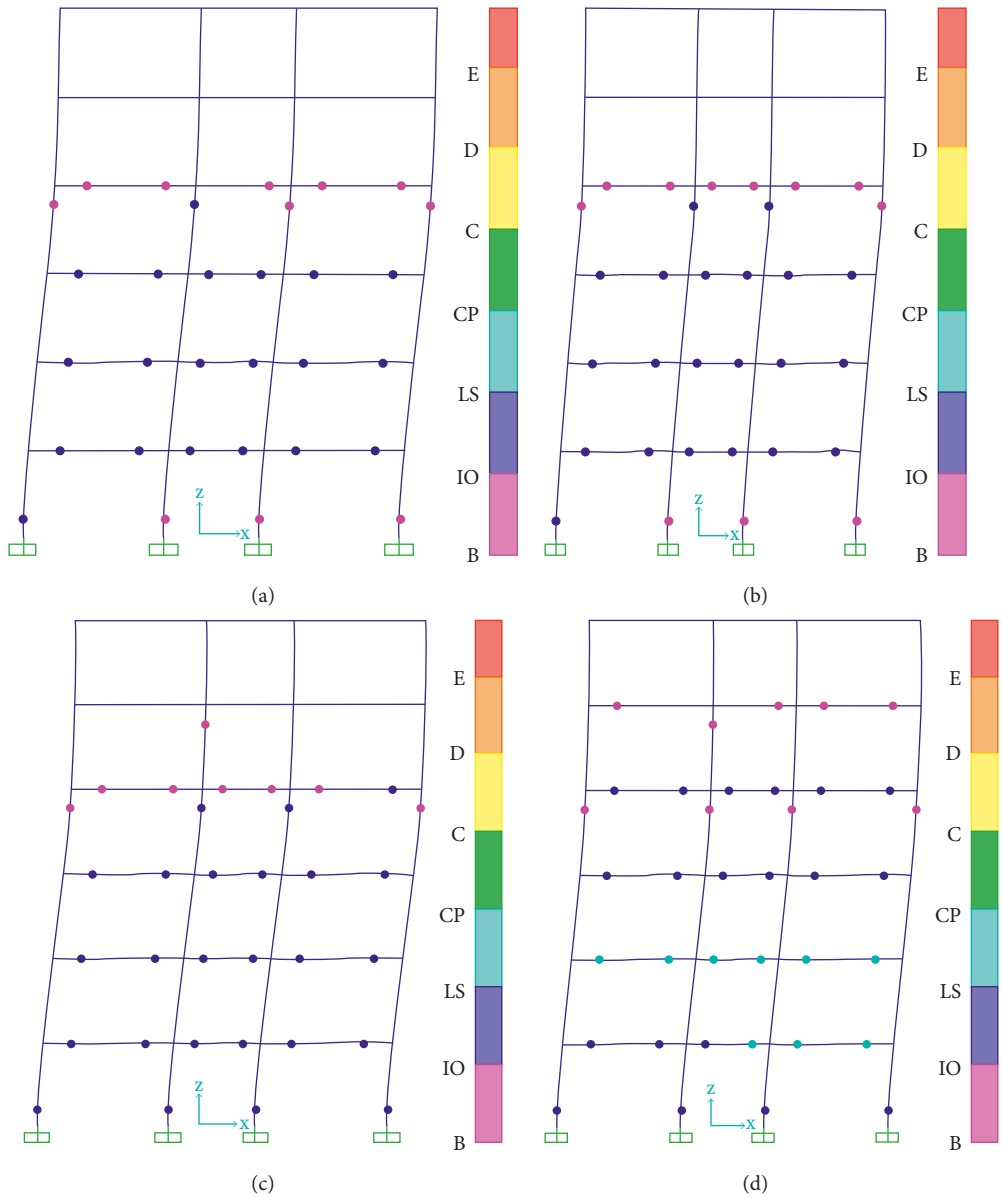

Figure 8: Distribution of plastic hinges under the 1st modal load pattern. (a) 0% corrosion rate. (b) 5% corrosion rate. (c) 10% corrosion rate. (d) 18% corrosion rate.

4.2.2. Degradation of the Seismic Performance of the Corroded Structure under Rare Earthquake Action. Figure 9 provides the pushover curves for the corroded frame under different degrees of corrosion. It is easy to see that the trend of the pushover curves and the degradation laws are basically the same despite the slight difference of the curves under different lateral load patterns. Table 9 lists the values of seismic bearing capacity of the frame under different corrosion rates. From the results in Figure 9 and Table 9, it can be concluded that the seismic bearing capacity of the corroded frame decreased significantly due to corrosion of its rebars. In addition, with increasing rebar corrosion rate, the degradation of the bearing capacity gradually increased.

4.2.3. Deformation Performance of the Corroded Structure under Rare Earthquake Action. In order to better understand the lateral deformation capacity of the corroded structure, this paper also provides the story drift ratios, as shown in Table 10. Similarly, we can see that the interstory drift ratios increase dramatically with the increasing of the corrosion rate of the structure. However, the increasing extent varies by floor position; for instance, there is a phenomenon of negative increase in the fifth and sixth floor, which is mainly caused by the redistribution of internal forces under different lateral load patterns.

Adding the interstory drift of each storey, one can get the storey displacements of the structure, which also represent the global behaviour of the corroded frame with stiffness and

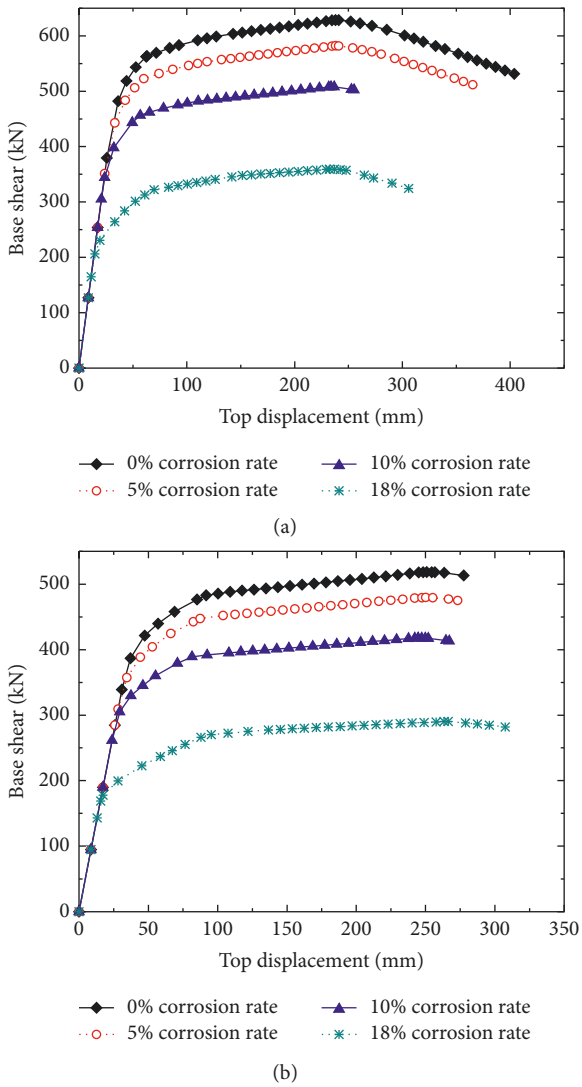

Figure 9: Comparison of the pushover curves of the corroded RC frame under different load patterns. (a) Under the uniform load pattern. (b) Under the 1st modal load pattern.

Table 9: Seismic bearing capacity of the corroded frame under rare earthquake action.

Corrosion rate (%)	Maximum base shear (kN)	
	Under the uniform load pattern	Under the 1st modal load pattern
0.0	628.5	518.5
5.0	581.9	479.6
10.0	508.1	417.7
18.0	359.2	290.3

ductility. Figure 10 reveals the storey displacements of the corroded structure under different lateral load patterns. The results indicate that the storey displacement increases with the increasing of corrosion rate. In addition, the deformation diagram of the frame is consistent with its 1st modal shape.

Table 10: Interstory drift ratios of the corroded frame structure.

Corrosion rate (%)		0.0	5.0	10.0	18.0
(a) Under the uniform load pattern					
Storey	1	1/163.9	1/156.3	1/142.7	1/127.9
	2	1/126.1	1/120.9	1/111.4	1/86.5
	3	1/148.6	1/140.1	1/125.2	1/79.9
	4	1/221.7	1/208.3	1/185.2	1/87.8
	5	1/565.0	1/574.7	1/598.8	1/138.3
	6	1/1219.5	1/1298.7	1/1449.3	1/689.7
(b) Under the 1st modal load pattern					
Storey	1	1/201.6	1/186.6	1/161.0	1/127.9
	2	1/126.6	1/119.6	1/108.1	1/86.5
	3	1/119.6	1/113.6	1/102.7	1/79.9
	4	1/140.3	1/132.6	1/119.2	1/87.8
	5	1/380.2	1/392.2	1/377.4	1/138.3
	6	1/888.0	1/934.6	1/1030.9	1/689.7

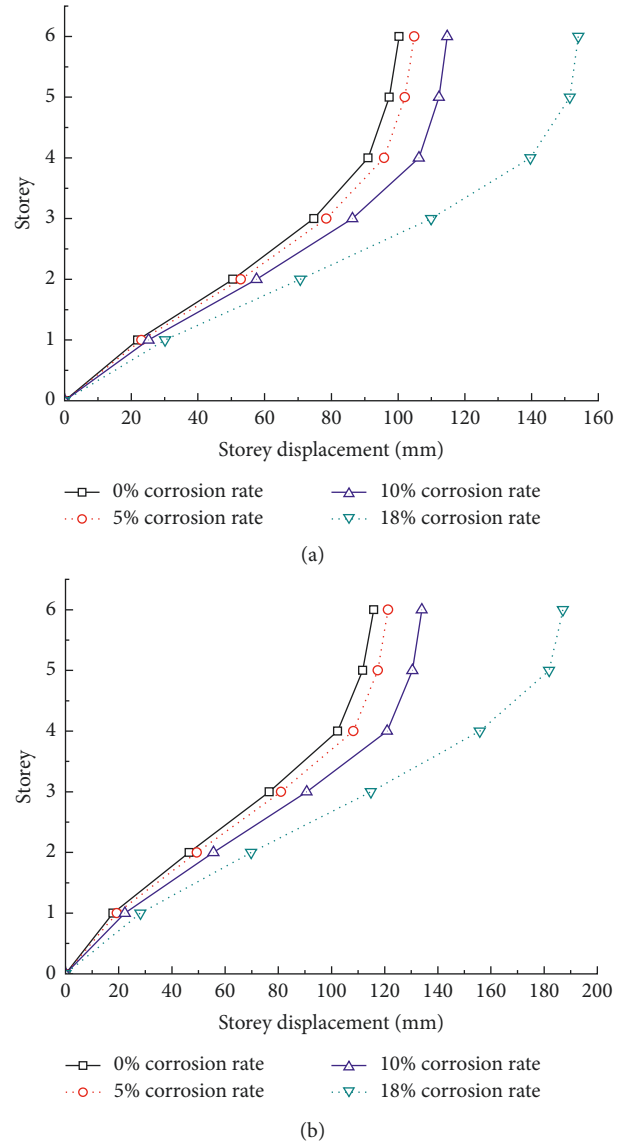

Figure 10: Comparison of the story displacements under different degrees of corrosion. (a) Under the uniform load pattern. (b) Under the 1st modal load pattern.

5. Conclusions

In this paper, the finite element model of a six-storey-three-span corroded reinforced concrete (RC) frame structure was established using SAP2000 software. The numerical simulation of the seismic performance of the corroded RC frame structure with four different amounts of corrosion was conducted using pushover analysis method. The main conclusions are as follows:

(1) For the noncorroded RC frame, the P-M-M curves of column section obtained by using user-defined hinges with the help of XTRACT software are generally consistent with those acquired by the built-in default hinges in SAP2000. For the corroded RC frame column section, the calculated P-M-M curves based on user-defined hinges present out the same change trends as the noncorroded one. Therefore, XTRACT software can be utilized to determine the properties of user-defined P-M-M plastic hinges.

(2) With the increasing corrosion rate of rebars, the plastic hinges in beams and columns of the RC frame developed rapidly from the bottom to the higher storey with an increasing development level, which leads to a more aggravated deformation of the structure under severe earthquake.

(3) The seismic bearing capacity of the corroded frame decreased significantly due to corrosion of its rebars. In addition, with increasing rebar corrosion rate, the degradation of the bearing capacity gradually increased.

(4) The interstory drift ratios increase dramatically with the increase of the corrosion rate of the structure. However, the increase varies with by the location of storeys, and it has a strong correlation with the lateral load pattern.

Conflicts of Interest

The authors declare that there are no conflicts of interests regarding the publication of this paper.

Acknowledgments

This research has been funded by the Outstanding Young Talent Research Fund of Zhengzhou University (Grant no. 1521322004) and Guangdong Provincial Key Laboratory of Durability for Civil Engineering, Shenzhen University (Grant no. GDDCE 12-06) and Foundation for University Young Key Teacher by Henan Province (Grant no. 2015GGJS-151).

References

[1] Z. Peng and L. Qingfu, "Effect of polypropylene fibre on mechanical and shrinkage properties of cement-stabilised macadam," *International Journal of Pavement Engineering*, vol. 10, no. 6, pp. 435–445, 2009.

[2] S. J. Kim and A. S. Elnashai, "Characterization of shaking intensity distribution and seismic assessment of RC buildings for the Kashmir (Pakistan) earthquake of October 2005," *Engineering Structures*, vol. 31, no. 12, pp. 2998–3015, 2009.

[3] R. Jünemann, J. C. de la Llera, M. A. Hube, L. A. Cifuentes, and E. Kausel, "A statistical analysis of reinforced concrete wall buildings damaged during the 2010, Chile earthquake," *Engineering Structures*, vol. 82, pp. 168–185, 2015.

[4] B. Zhao, F. Taucer, and T. Rossetto, "Field investigation on the performance of building structures during the 12 May 2008 Wenchuan earthquake in China," *Engineering Structures*, vol. 31, no. 8, pp. 1707–1723, 2009.

[5] Y. G. Du, L. A. Clark, and A. H. C. Chan, "Residual capacity of corroded reinforcing bars," *Magazine of Concrete Research*, vol. 57, no. 3, pp. 135–147, 2005.

[6] F. J. Molina, C. Alonso, and C. Andrade, "Cover cracking as a function of rebar corrosion: part II—numerical model," *Materials and Structures*, vol. 26, no. 9, pp. 532–548, 1993.

[7] X. G. Wang, W. P. Zhang, X. L. Gu, and H. C. Dai, "Determination of residual cross sectional areas of corroded bars in reinforced concrete structures using easy-to-measure variables," *Construction and Building Materials*, vol. 38, pp. 846–853, 2013.

[8] A. N. Kallias and M. L. Rafiq, "Finite element investigation of the structural response of RC beams," *Engineering Structures*, vol. 32, no. 9, pp. 2984–2994, 2010.

[9] P. Zhang and Q. F. Li, "Experimental study on shrinkage properties of cement-stabilized macadam reinforced with polypropylene fiber," *Journal of Reinforced Plastics and Composites*, vol. 29, no. 12, pp. 1851–1860, 2010.

[10] G. Zhao, M. Zhang, Y. Li, and D. Li, "The hysteresis performance and restoring force model for corroded reinforced concrete frame columns," *Journal of Engineering*, vol. 2016, Article ID 7615385, 19 pages, 2016.

[11] O. Trocónis de Rincón and D. Colaboration, "Durability of concrete structures: DURACON, an iberoamerican project. Preliminary results," *Building Environment*, vol. 41, no. 7, pp. 952–962, 2006.

[12] H. Yalciner, S. Sensoy, and O. Eren, "Time-dependent seismic performance assessment of a single-degree-of-freedom frame subject to corrosion," *Engineering Failure Analysis*, vol. 19, pp. 109–122, 2012.

[13] S. Pour-Ali, C. Dehghanian, and A. Kosari, "Corrosion protection of the reinforcing steels in chloride-laden concrete environment through exoxy/polyaniline-camphorsulfonate," *Corrosion Science*, vol. 90, pp. 239–247, 2015.

[14] D. E. Choe, P. Gardoni, D. Rosowsky, and T. Haukaas, "Probabilistic capacity models and seismic fragility estimates for RC columns subject to corrosion," *Reliability Engineering and System Safety*, vol. 93, no. 3, pp. 383–393, 2008.

[15] L. Berto, R. Vitaliani, A. Saetta, and P. Simioni, "Seismic assessment of existing RC structures affected by degradation phenomena," *Structural Safety*, vol. 31, no. 4, pp. 284–297, 2009.

[16] L. Berto, A. Saetta, and P. Simioni, "Structural risk assessment of corroding RC structures under seismic excitation," *Construction and Building Materials*, vol. 30, pp. 803–813, 2012.

[17] E. A. P. Liberati, C. G. Nogueira, E. D. Leonel, and A. Chateauneuf, "Nonlinear formulation based on FEM, Mazars damage criterion and Fick's law applied to failure assessment of reinforced concrete structures subjected to chloride ingress and reinforcements corrosion," *Engineering Failure Analysis*, vol. 46, pp. 247–268, 2014.

[18] Computers and Structures Inc. (CSI), *SAP2000. Three Dimensional Static and Dynamic Finite Element Analysis and Design of Structures V16.0.2*, Computers and Structures Inc., Berkeley, CA, USA, 2013.

[19] A. Koçak, B. Zengin, and F. Kadioğlu, "Performance assessment of irregular RC buildings with shear walls after earthquake," *Engineering Failure Analysis*, vol. 55, pp. 157–168, 2015.
[20] SAP2000, *Integrated Finite Element Analysis and Design of Structure: Analysis Reference*, Computers and Structures, Inc., Berkeley, CA, USA, 2000.
[21] ATC-40, *Seismic Evaluation and Retrofit of Concrete Buildings*, Applied Technology Council, Redwood City, CA, USA, 1996.
[22] I. Khan, R. Francois, and A. Castel, "Prediction of reinforcement corrosion using corrosion induced cracks width in corroded reinforced concrete beams," *Cement and Concrete Research*, vol. 56, pp. 84–96, 2014.
[23] J. Rodriguez, L. M. Ortega, and J. Casal, "Load carrying capacity of concrete structures with corroded reinforcement," *Construction and Building Materials*, vol. 11, no. 4, pp. 239–248, 1997.
[24] G. H. Xing and D. T. Niu, "Analytical model of flexural behavior of corroded reinforced concrete beams," *Journal of Central South University (Science and Technology)*, vol. 45, no. 1, pp. 193–201, 2014.
[25] D. Coronelli and P. Gambarova, "Structural assessment of corroded reinforced concrete beams: modeling guidelines," *Journal of Structural Engineering*, vol. 130, no. 8, pp. 1214–1224, 2004.
[26] S. Han and P. Johanne, "Mechanistic study on the effect of sulfate ions on polycarboxylate superplasticisers in cement," *Advances in Cement Research*, vol. 25, no. 4, pp. 200–207, 2013.
[27] W. L. Jin and J. Xia, "Influence of pitting corrosion o-n the bending capacity of reinforced concrete beams," *Building Structures*, vol. 39, no. 4, pp. 100–111, 2009.
[28] X. H. Wang and X. L. Liu, "Modeling the flexural carrying capacity of corroded RC beam," *Journal of Shanghai Jiaotong University*, vol. 13, no. 2, pp. 129–135, 2008.
[29] Q. Wu and Y. S. Yuan, "Experimental study on the deterioration of mechanical properties of corroded steel bars," *China Civil Engineering Journal*, vol. 41, no. 12, pp. 42–47, 2008.
[30] GB50011, *Code for Seismic Design of Buildings. National Standard of P. R. China*, China Architecture & Beijing Press, Beijing, China, 2010.
[31] GB50009, *Load Code for the Design of Building Structures. National standard of P. R. China*, China Architecture & Beijing Press, Beijing, China, 2012.
[32] FEMA-356, *Prestandard and Commentary for the Seismic Rehabilitation of Buildings*, American Society of Civil Engineers, Reston, Virginia, USA, 2000.
[33] C. D. Comartin, R. W. Niewiarowski, S. A. Freeman, and F. M. Turner, "Seismic evaluation and retrofit of concrete buildings: a practical overview of the ATC 40 document," *Earthquake Spectra*, vol. 16, no. 1, pp. 241–261, 2000.
[34] XTRACT, *Cross Section Analysis Program for Structural Engineers*, IMBSEN & Associates Inc., Sacramento, CA, USA, 2007.
[35] Y. L. Li, *Analysis for Seismic Performance of Corroded RC Frame Structures*, Zhengzhou University, Zhengzhou, China, 2016.